Tropical tree diversity enhances light capture through crown plasticity and spatial and temporal niche differences

Jurgis Sapijanskas, Alain Paquette, Catherine Potvin, Norbert Kunert and Michel Loreau

Appendix C: Light interception model.

This appendix describes the spatially explicit light interception model we developed. It was adapted from the light module implemented in SORTIE (Canham *et al.*, 1999) in order to incorporate phenological differences among species and micro-topography, that is small variations in soil elevation, thanks to a digital elevation model (Wolf et al., 2011). Our model also granted more flexibility in the crown radius and crown depth allometric relationships. Finally, it enabled us to implement an optimization scheme using light availability data to inform 'Crown Openness' (CO), for which much uncertainty lies in the empirical protocol followed to estimate it (Boivin *et al.*, 2011). The light model predicts light conditions in terms of the gap light index (GLI) as a function of (i) the spatial location, (ii) size and species identities of trees in the vicinity, and (iii) local solar and meteorological parameters.

Model description

Trees are represented as semi-opaque cylinders characterised by their spatial location (x,y,z), radius, base, top and a species-specific "crown openness" (CO, ranging in $[0, 1]$). Our plantation was

mapped and a digital elevation model (Wolf et al., 2011) was used to estimate elevation (z) for every tree. The top of the cylinder was set as the height of the tree as measured annualy in the field. The base and radius of the cylinder were obtained from species-specific empirical relationships established from data collected in the plantation (see below). Similar to SORTIE, it is assumed that species-specific fractions of incident light (CO) are transmitted through a tree's crown.

In order to calculate the amount of light reaching a specific location, the model simulates taking a fisheye photograph from that position to determine which parts of the sky are blocked by taller trees nearby. The differences among sky regions in the amount of radiation they conceal is then taken into account to compute the total light in any point. For any given location, the model divides the sky hemisphere above that point into 10,000 equal-area regions. The total incident photosynthetically active radiation (PAR) originating from each region over a specified amount of time is calculated by tracking the sun's position at 5-minute intervals throughout that period. Diffuse radiation is assumed to be isotropic and its percentage relative to direct beam radiation depends on atmospheric parameters. The only modification we brought to the sky hemisphere calculations compared to SORTIE was to make all atmospheric parameters change over time with a monthly resolution. Thanks to reduced cloud cover, daily PAR indeed varies throughout the year and is notably ca. 50% higher in the dry season than in the wet season (Kunert et al, 2011). We used 30-year normals from the closest weather station located at Barro Colorado Island (BCI) to estimate the spectral (PAR over irradiance) and direct beam fractions every month for our plantation.

The openness of each sky region is calculated as the product of the openness of crowns that blocks the sky in that direction. The openness of a sky region where no trees are present is thus 1. Each region's openness is then multiplied by the region's total PAR and then summed over all sky regions over a certain minimum solar angle. The result is then divided by the total PAR

that would reach the focal point if they were no neighbouring trees to obtain the gap light index (GLI). It is assumed that no light comes from sky regions below a minimum solar angle because of surrounding obstacles, would it be vegetation, soil or buildings. The model was implemented in the Java programming language.

Parametrization

Allometric models of crown radius and crown depth

While the top of the crown was set as measured tree height, empirical relationships were used to relate tree size and both the base and radius of the crown. Over 2010 and 2011, 584 trees were sampled (more than 109 per species except Ca, the species that failed to establish, for which 29 out of the 51 remaining individuals were sampled) to establish species-specific allometric relationships of crown radius *rad* and crown depth *dep*. Our data included 4 measurements per individual tree: diameter at ground level BD; Number of stems N_{stem}; basal area summed over the N_{stem} stems BA and height H. Contrary to most studies, bookkeeping in the Sardinilla plantation is done on a per individual, and not stem-by-stem, basis such that trees can have multiple stems. With the factors *plot* and diversity treatment (*div*, either monoculture, 3- or 6-species mixture), we had 5 potential variables to build predictive allometric relationships from.

Controlling for plot effects, diversity effects on both dimensions of crown size were detected (Tables C1 and C2) so that *div* had to be taken into account. Model comparisons based on AICc revealed strong model selection uncertainty in that no 'best' model could be clearly identified. We thus applied a modelling averaging approach (Burnham & Anderson, 2002) that we implemented with the glmulti package (Calcagno & de Mazancourt, 2010) of R. For all species except Ca, we treated plot as a random effect and considered all linear mixed models of crown depth that could be formed with the factors N_{stem} and *div*, the covariates BA, BD and H and the all the two-way

interaction between a factor and a covariate. A power law was more appropriate for crown radius so that all models of log-transformed crown radius that could be derived with the two factors, the log-transformed covariates and the two-way interactions between a factor and a log-transformed covariate were considered. Each model m was fit with the lme4 package of R and its Akaike weight w_m was computed as $w_m = \frac{e^{-0.5\Delta_m}}{\sum_k e^{-0.5\Delta_k}}$ where $\Delta_m = AICc_m - \min\{AICc\}$ is the AICc difference between m and the 'best' candidate model. Finally, for each tree i, the weighted average of crown radius ($\log rad_{i,m}$) and depth ($dep_{i,m}$) predicted by each model m was computed to produce unconditional predictions $\log rad_i = \sum_m w_m \log rad_{i,m}$ and $dep_i = \sum_m w_m dep_{i,m}$ accounting for model selection uncertainty. Results were satisfactory (Figure C1) and captured architectural differences among species (Table C3)

Table C1. Diversity effects on crown radius. Plot was treated as a random effect. *BA* designates basal area and *div* is a factor coding for diversity treatement: either monoculture, 3- or 6-species mixture. P values were obtained by likelihood ratio tests. Ca was not considered since it was not present in monoculture.

	Chisq	df	P value
species	50.831	4	2.42E-10
species $\times \log BA$	800	5	<2.2E-10
species $\times$ *div*	20.669	10	0.024

Table C2. Diversity effects on crown depth. Same as Table C1 with crown depth instead of the log-transformed crown radius as a response variable.

	Chisq	df	P value
species	117.43	4	<2.2E-10
species $\times H$	1074.7	5	<2.2E-10
species $\times$ *div*	21.192	10	0.020

Crown openness

Our light model, like SORTIE, assumes that a species-specific fraction of incident light, called crown openness (CO), is transmitted through a tree's crown. According to the way we modeled

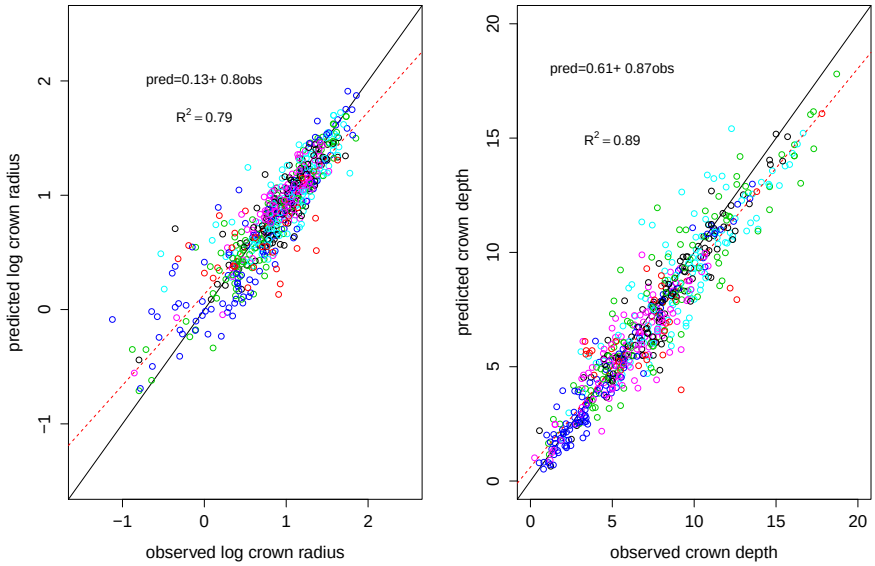

Fig. C1. Allometric models prediction plotted against observation for log crown radius (m) and crown depth (m).

Table C3: Average tree size in 2009 (m).

Species	Ae	Ca	Co	Hc	Ls	Tr
Height	7.1	7.9	9.0	4.8	8.7	6.8
Crown radius	2.1	1.3	1.9	1.6	2.3	2.4
Crown depth	6	4.9	6.2	3.2	7.3	4.8

phenology, we estimated a pair of CO for each species corresponding to fully-foliated and leafless periods.

For the fully-foliated period, we first estimated CO from the September hemispherical photographs where single tree crowns could be outlined, that is where the entire crown of a tree could be singled out and was not overlapping with other trees (8 to 24 crowns per species). Following standard protocol (Canham *et al.*, 1999) , CO was measured as the fraction of sky visible through the crown. Results (Table C4) confirmed that much uncertainty lied in the choice of the crown outline (Boivin *et al.*, 2011). We thus implemented an optimization scheme using light availability data to estimate the CO that best captured the shading effect of crowns modelled as cylinders.

Calibrated CO values were obtained thanks to simulated annealing, a global optimization procedure (Goffe *et al.*, 1994), using the summed squared error between observed and modelled GLI as the objective function. Our optimization scheme has some similarities with the methods initially used by Canham *et al.* (1994) to parametrize an analogous light model. Alternatively, September hemispherical photographs from all subplots, monoculture subplots only or mixture subplots only were used in the optimization procedure but they all provided similar CO values (less than 4% differences far all species) so that only CO values using all September hemispherical photographs are reported since it makes use of all the information we have to inform CO estimation. This indicates that either there was no diversity effects on CO or that our methods are not precise enough to detect it. Calibrated CO values lied within the 95% confidence intervals of the empirical estimates using a rectangular outline (Table C4).

Table C4. Estimates of crown openness when trees are fully foliated. 'Outline' columns corre- spond to estimates obtained from hemispherical photograph of individual tree crowns analyzed with Crown Delineator (Boivin *et al.*, 2011) with different outlines. The outlines were a geometri- cal outline corresponding to the trace that would leave the edge of a 20 pixel radius "moving disk" circling the crown (20), the smallest smallest convex polygon encompassing the crown (CH, convex Hull algorithm) or the smallest rectangle including the crown (rect). Calibrated values were ob- tained thanks to a global optimization procedure using the summed squared error between observed and predicted GLI as the objective function. *Light data from hemispherical photograph poorly constrained the crown openness of the species that failed to establish (Ca) so that it could not be uniquely determined by optimization. Since all small values were equivalent, the corresponding crown openness was set to zero.

Species	Crown Openness			
	Outline 20	Outline CH	Outline rect	Calibrated
Ae	0.18± 0.03	0.40 ± 0.07	0.58 ± 0.09	0.64
Ca				0*
Co	0.20 ± 0.07	0.49 ± 0.08	0.64 ± 0.07	0.76
Hc	0.31 ± 0.09	0.59 ± 0.12	0.72 ± 0.09	0.77
Ls	0.18 ± 0.06	0.42 ± 0.04	0.59 ± 0.04	0.64
Tr	0.25 ± 0.07	0.45 ± 0.09	0.63 ± 0.09	0.73

We estimated the CO of leafless trees (Tab. C5) with three sets of hemispherical photographs from distinct phenological periods (Fig. 2 in the main text). These were 20, 35 and 36 photographs

taken on December, 25th 2007, March, 21st 2008 and June, 17th 2008. We used the same optimisation scheme as before. For each set of photographs, the CO of species modeled as fully-foliated in that period were fixed to the values estimated from the September photographs (Tab. C4). We estimated CO for Ae in periods 3 and 4 (Fig. 2) from the December pictures with one free parameter for 20 observations. The CO of Co in phenological periods 1, 4, 5 and 6 as well as the CO of Hc in periods 3 to 5 were estimated from the March pictures. Finally, we used the June photographs for the CO of Ls in periods 1 and 6 and the CO of Tr in period 1.

Table C5. Estimates of crown openness when trees are leafless.

Species	Leafless crown openness
Ae	0.85
Co	0.95
Hc	0.93
Ls	0.90
Tr	0.97

Validation

All the parameters of the light model except crown openness (CO), which is the parameter that has the least effect on predictions (Beaudet *et al.*, 2002), are derived from independent empirical measurements (tree height, crown depth, crown radius, phenology). To avoid circularity, validation was carried out by regressing GLI observations and GLI predictions by the light model for monoculture subplot (respectively mixture subplots) using CO values obtained with our optimization procedure using mixtures subplots (respectively monoculture subplots) only. In both cases, predictions of the light interception model were closely related to observed GLI values with a relationship not significantly different from identity. The regression between independent predictions of GLI and observations in monocultures had a slope of 0.87 ± 0.09 and an intercept of 7.51 ± 4.79 ($R^2 = 0.72$, Fig. C2). The regression between simulated and observed values was even closer to identity when

considering mixture plots only (slope 0.99 ± 0.09 and intercept -1.42 ± 3.89, $R^2 = 0.75$). As for the CO values, GLI predictions were not sensitive to the set (monoculture subplots or mixtures subplots only) of hemispherical photographs used in optimization procedure (Fig. C4), which confirms that the type of light model we used are not too sensitive to CO values (Beaudet *et al.*, 2002). In any case, this result allowed us to use CO values obtained when using all hemispherical photographs for calibration (Tab. C4) in the rest of our work.

Using these CO values, the regression of predictions against observations yielded a relationship not significantly different from identity (slope 0.95 ± 0.06 and intercept 1.84 ± 2.97, $R^2 = 0.75$; Fig. C5). In all cases (circular and non circular predictions), the absence of bias ensures that systematic deviations between observed and simulated values in bootstrap tests are not due to the light model. Diversity, measured as plot-level species richness, did not explain deviations of observations from model predictions (Table C6). There was no miscalibration that might have produced 'false' diversity effects in the subsequent tests and, reciprocally, our light interception model captured the most important aspects that may contribute to diversity effects on community-level light capture, namely, overyielding, differences in architecture among species and/or plastic changes in crown geometry. The model error (Fig. C5), while non negligible, compares advantageously with other uses of this type of model (e.g., Beaudet *et al.*, 2002). Moreover, this error, since it is non biased, adds noise that contributes to mask diversity effects on light capture and hence makes our tests conservative.

Table C6. ANCOVA of observed GLI. No effect of diversity measured by plot species richness. 'diversity' was coded as a 3-level factor: monoculture, 3-species mixture or 6-species mixture.

	Df	Sum Sq	Mean Sq	F value	Pr(>F)
Predicted GLI	1	27418.46	27418.46	255.25	$< 2E-16$
diversity	2	131.88	65.94	0.61	0.5437
Residuals	81	8700.71	107.42		

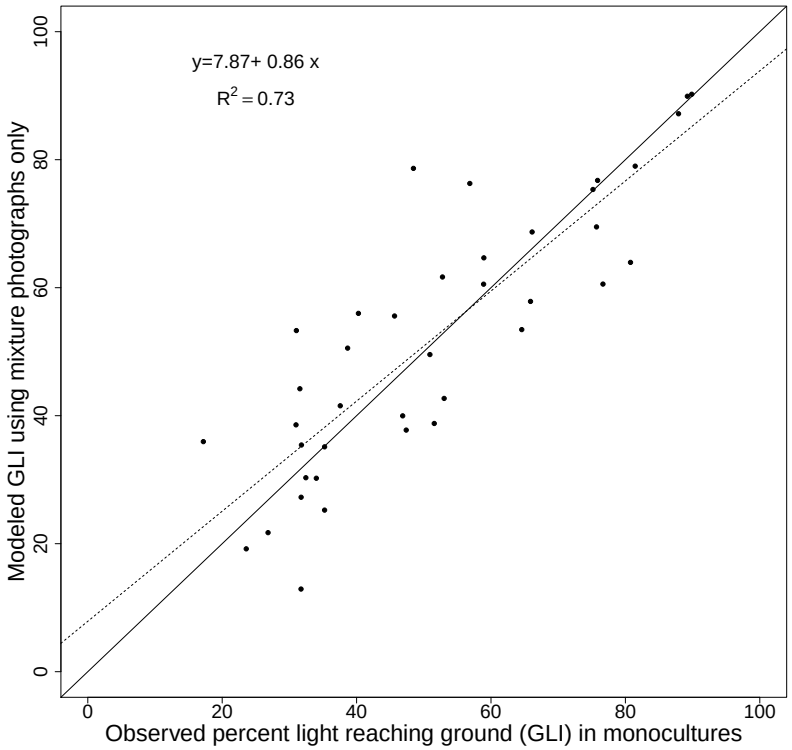

Fig. C2. Model validation: predictions of the light model using CO estimated from monoculture hemispherical photographs only plotted against predictions using CO estimated from mixtures hemispherical photographs only. Symbols are GLI at subplot center. Red: mixture subplots. Black: monoculture subplots. The dotted line shows the linear fit.

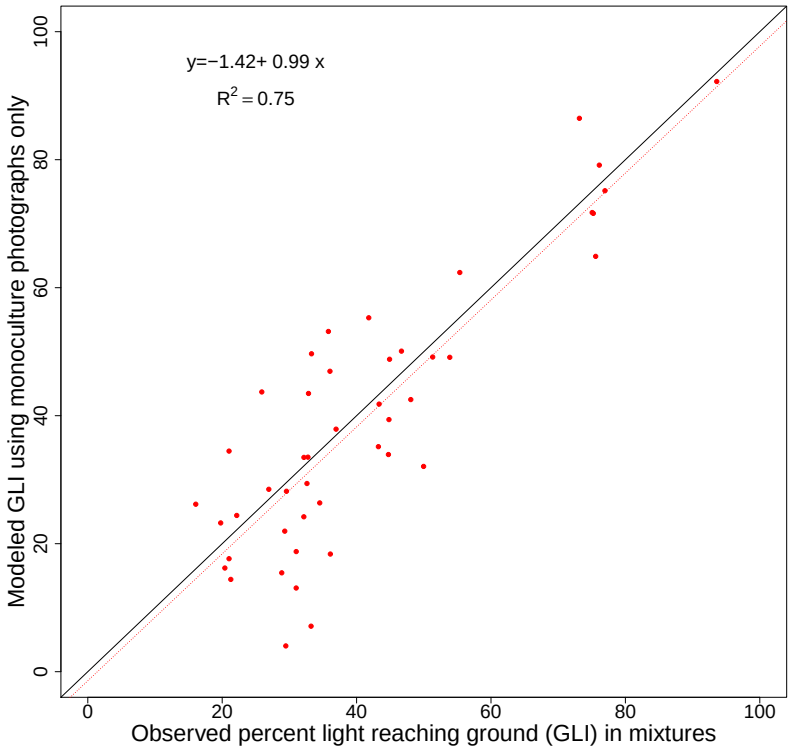

Fig. C3. Model validation: predictions of the light model using CO estimated from mixture hemispherical photographs only plotted against predictions using CO estimated from monoculture hemispherical photographs only. Symbols are GLI at subplot center. Red: mixture subplots. Black: monoculture subplots. The dotted line shows the linear fit.

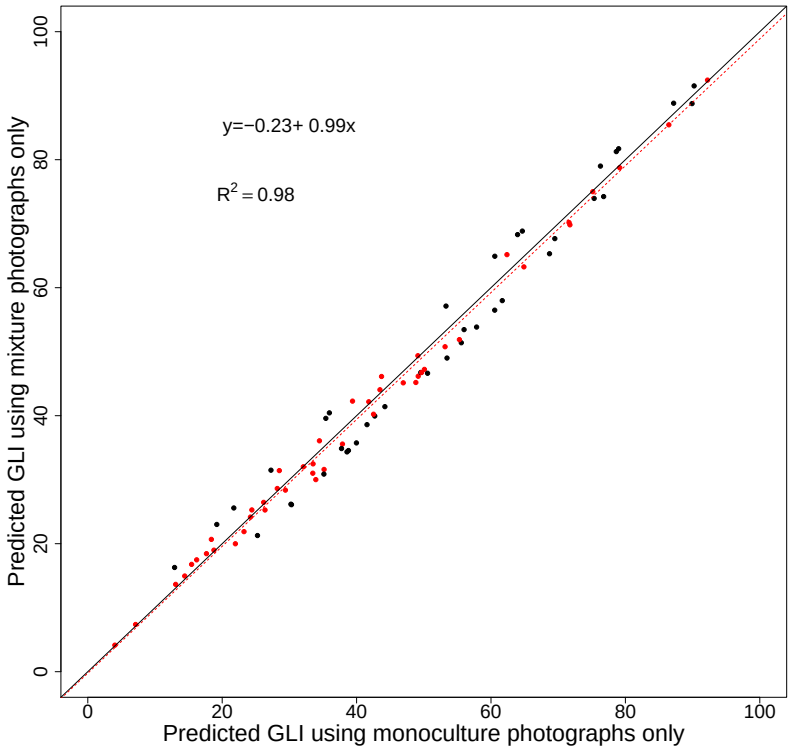

Fig. C4. Model sensitivity to CO values. Predictions of the light model using CO estimated from mixture hemispherical photographs only plotted against predictions using CO estimated from monoculture hemispherical photographs only. Symbols are GLI at subplot center. Red: mixture subplots. Black: monoculture subplots. The dotted line shows the linear fit.

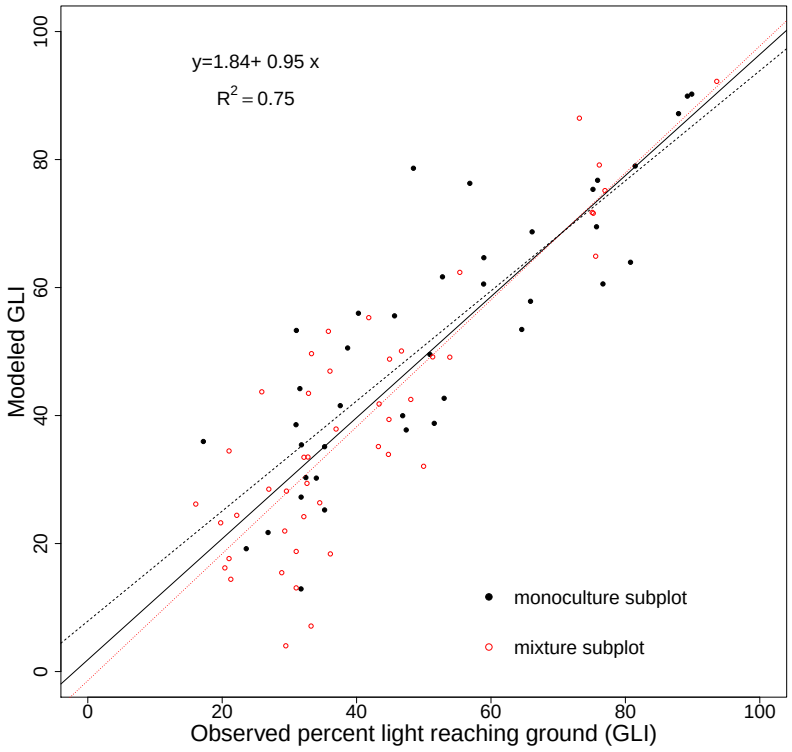

Fig. C5. Predictions from the light model plotted against observations of percent light reach- ing ground (GLI) at the center of 85 subplots using CO values obtained using all hemispherical photographs. 3 of the 88 subplots were removed because low branches obscured the hemispherical photographs and biased the light measure. The continuous black, black-dashed and dotted-red lines are linear regression fits when considering all, only monoculture and only mixture subplots, respectively.

Literature cited

Beaudet, M., Messier, C. & Canham, C.D. (2002). Predictions of understorey light conditions in northern hardwood forests following parameterization, sensitivity analysis, and tests of the sortie light model. *Forest Ecology and Management*, 165, 235–248.

Boivin, F., Paquette, A., Racine, P. & Messier, C. (2011). A fast and reliable method for the delineation of tree crown outlines for the computation of crown openness values and other crown parameters. *Canadian Journal of Forest Research-Revue Canadienne De Recherche Forestiere*, 41, 1827–1835.

Burnham, K. & Anderson, D. (2002). *Model selection and multimodel inference: a practical information-theoretic approach*. 2nd edn. Springer.

Canham, C.D., Coates, K.D., Bartemucci, P. & Quaglia, S. (1999). Measurement and modeling of spatially explicit variation in light transmission through interior cedar-hemlock forests of british columbia. *Canadian Journal of Forest Research-Revue Canadienne De Recherche Forestiere*, 29, 1775–1783–.

Canham, C.D., Finzi, A.C., Pacala, S.W. & Burbank, D.H. (1994). Causes and consequences of resource heterogeneity in forests - interspecific variation in light transmission by canopy trees. *Canadian Journal of Forest Research-Revue Canadienne De Recherche Forestiere*, 24, 337–349.

Goffe, W., Ferrier, G. & Rogers, J. (1994). Global optimization of statistical functions with simulated annealing. *Journal of Econometrics*, 60, 65–99.